

Angular distributions for H^- formation in single collisions of H^+ on Mg

I. Alvarez and C. Cisneros

Instituto de Fisica, Universidad Nacional Autonoma de Mexico, Mexico 20, Distrito Federal

A. Russek

Department of Physics, The University of Connecticut, Storrs, Connecticut 06268

(Received 4 January 1982)

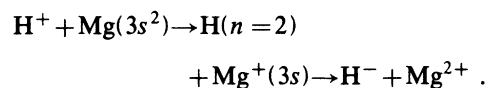
Absolute differential cross sections have been measured for H^- formation in single collisions of H^+ on Mg in the energy range from 0.5 to 5.0 keV. Total cross sections, obtained by direct integration of these differential cross sections, are in good agreement with earlier total-cross-section measurements of Morgan and Eriksen in the energy range common to the two experiments and are in good agreement with the calculated total cross sections of Olson and Liu. The differential cross sections are strongly peaked in the forward direction. The functional form and scaling properties of this forward peak strongly indicate that it is a glory maximum, which occurs when the classical deflection function changes over from attractive to repulsive at some finite impact parameter. The differential cross sections from 1.0 to 5.0 keV show no other structure, but below 1.0 keV a τ -dependent structure is observed which becomes more pronounced as the collision energy decreases.

MS code no. AN2003 1977 PACS numbers: 34.70. + e, 34.10. + x

I. INTRODUCTION

Total cross sections for charge-changing processes of H^+ on Mg have been obtained by Berkner, Pyle, and Stearns¹ at collision energies 5–70 keV and by Morgan and Eriksen^{2,3} at energies 1–100 keV. Insofar as the process $H^+ + Mg \rightarrow H^- + Mg^{2+}$ is concerned, Olsen and Liu⁴ have suggested that a high-energy maximum in the total-cross-section data of Morgan and Eriksen can be attributed to the $H^+ + Mg(3s^2)$ incident channel passing diabatically through a series of curve crossings on the inward portion of the trajectory and making a transition to the $H^- + Mg^{2+}$ curve on the repulsive wall of the potentials. They further attribute the low-energy behavior to a transition at the avoided crossing between the incident $H^+ + Mg(3s^2)$ and the $H + Mg^+(4s)$ curves on the outward portion of the trajectory followed by a series of transitions at curve crossings which lead to $H^- + Mg^{2+}$. Such speculations on the dynamics of transitions at level crossings which occur during the collision process are made necessary by the limited amount of information contained in total-cross-section data. It was therefore felt that a better understanding of the physical processes could be obtained by studying differential cross sections as well as total cross sections. With this motivation, differential cross sections are reported here for the process $H^+ + Mg \rightarrow H^- + Mg^{2+}$ at energies 0.5–5.0 keV. These differential-cross-section measurements do

not bear out the interpretations of Olson and Liu concerning the high-energy maximum in the total-cross-section data of Morgan and Eriksen. In the energy range from 2.0 to 5.0 keV, the angular distributions are quite smooth, with no hint at any transitions taking place at any nonzero value of $\tau = E\theta$. In particular, there is no hint of any transition on the repulsive wall of the potentials. On the other hand, the low-energy differential-cross-section measurements do exhibit τ -dependent structures which could be attributed to a transition at the $H^+ + Mg(3s^2)$ and $H + Mg^+(4s)$ curve crossing, as Olson and Liu suggest, although the observed τ value for this transition suggests the sequence



The most interesting feature of the angular distributions, however, is a clear indication of a glory maximum at a 0° scattering angle. This arises because the deflection function⁵ $\theta(b)$ passes through 0° as it changes from negative (attractive scattering at large impact parameter) to positive (repulsive scattering at small impact parameter).

It will be shown that the quantum-mechanical model of Ford and Wheeler⁶ predicts a universal curve for glory scattering if $E^{-3/2}d\sigma/d\omega$ is plotted as a function of $E\theta$. The measured angular distribution are much better represented by these reduced variables than they are by the conventional ρ -vs- τ

reduced variables, particularly at the higher collision energies.

A final contribution of this work is the introduction of a scaling law which is fully equivalent to the ρ -vs- τ scaling law introduced by Smith *et al.*,⁷ yet exhibits the shape of the differential cross section. It is shown that if the scattering force and excitation probability depend on position only (and not on velocity), then $E^{-2}d\sigma/d\omega$, when plotted as a function of $\tau = E\theta$ should yield a universal curve just as does the $\rho = (\theta \sin\theta d\sigma/d\omega)$ -vs- τ plot. The utility of the new plot introduced here stems from the fact that the $(E^{-2}d\sigma/d\omega)$ -vs- $E\theta$ universal curve has the shape of the differential cross section, which the ρ -vs- τ plot does not. The new plot is particularly important in this work, because the shape of the differential cross section in the vicinity of 0° is the crux of the present study. A ρ -vs- τ plot would be useless in this angular region.

II. APPARATUS AND MEASUREMENTS

The experimental arrangement shown in Fig. 1 is essentially the same as described in a previous paper⁸ and consists basically of three parts: ion source, collision chamber, and detection system. An H^+ beam is produced by a colutron-type ion source, part of a 5-keV accelerator of the Instituto de Fisica, Universidad Nacional Autonoma de Mexico. After acceleration and focusing, the H^+ ions are analyzed by a Wien velocity filter⁹ and bent 10° by cylindrical electrostatic deflection plates in order to prevent photons created in the ion source from reaching the detection system. This collimated and analyzed H^+ beam passes through the collision chamber, which houses an oven containing Mg vapor, where some of the H^+ ions capture electrons to form H^0 or H^- . After the interaction region, scattered ions and neutrals enter the detector chamber

which can rotate about the center of the oven, so that angular distributions of H^0 and H^- can be obtained. A retractable Faraday cup is placed between the Mg oven and the detector assembly to measure the total incoming beam. The entire system is evacuated by three diffusion pumps and a turbomolecular pump which maintain the pressure outside the collision chamber at around 10^{-7} torr. Typical working pressures are 5×10^{-6} in the source region, approximately 10^{-4} torr in the oven, and less than 3×10^{-7} torr in all other regions. The magnesium oven is essentially the same as that used in previous experiments¹⁰ for a Cs target. It is made of a stainless steel block 3.2 cm wide and 2.8 cm long.

The beam enters the collision cell through a 1-mm diameter aperture with a knife edge. The exit aperture was a 2×6 -mm² slit which permits measurements of scattered beam between -13° and 13° with respect to the beam axis in the horizontal plane. The magnesium reservoir is mounted by a screw connection to the bottom. The oven and reservoir are heated by two 150-W resistive heating elements placed in two cavities bored lengthwise in the stainless-steel block. Chromel-Alumel thermocouples are attached to the magnesium oven and to the reservoir to measure the respective temperatures. These thermocouples were calibrated at 273 and 373 K with an accuracy of approximately 0.5 K.

After the oven was loaded with magnesium (99.99% pure) it was outgassed at a high temperature for several hours before the data were taken. Typical working oven temperatures run from 575 to 600 K. The magnesium vapor density was calculated from available vapor-pressure data.¹¹⁻¹³ Vapor-pressure-versus-temperature data were taken from these papers and a curve fitted to the data points. The magnesium oven and reservoir were placed inside a water-cooled cylinder 12 cm in diameter in order to prevent magnesium vapor from

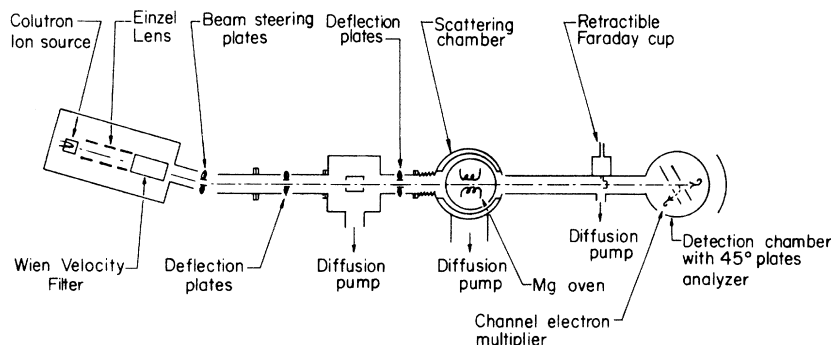


FIG. 1. Schematic diagram of the apparatus.

contaminating the vacuum system and detectors.

The detection system for the ions consists essentially of a parabolic 45° electrostatic analyzer with a funnel-type channel electron multiplier to measure the ions. The energy resolution of the analyzer was approximately 10% so that all ions within the distribution of energy losses were counted by one voltage setting of the electrostatic analyzer. An aperture was cut in the rear part of the analyzer so that the neutral beam could be simultaneously measured by a second channel electron multiplier. Since the total beam was measured by a Faraday cup, experimental data have been corrected for multiplier counting efficiency for H⁻ which has been measured before.¹⁴

In this experiment, as has been pointed out previously,¹⁰ the basic angular distributions are smeared owing to three factors: the angular and energy distribution of the beam entering the cell (θ_B), the finite resolution of the ion detection system (θ_D), and the finite size of the collision volume (θ_V). From the geometry the resolutions were calculated as follows: $\theta_B = 0.4$ mrad; $\theta_D = 0.6$ mrad; $\theta_V = 1.4$ mrad. The total resolution can be characterized by a root-mean-square resolution of 1.57 mrad (0.090°). Lengths and apertures have been changed from that reported in Ref. 10 in order to achieve better angular resolution.

The procedure was the same as described in Ref. 10. The total incident current I_0 was measured by a retractable Faraday cup. The H⁻ current $I^-(\theta)$, scattered into a solid angle $d\omega$, was determined as a function of θ as the detector assembly was rotated about the Mg oven center. The number of Mg atoms present in the scattering cell was determined from the cell temperature using the vapor-pressure-temperature tables and the differential cross section was obtained using the relation

$$\frac{d\sigma^-}{d\omega} = \frac{I^-(\theta)}{I_0 n l}, \quad (1)$$

where l is the effective path length and n is the Mg particle density. The total cross section is found by integration over angles θ and ϕ and, since the scattering is symmetrical about the scattering angle ϕ , gives

$$\sigma_- = 2\pi \int_0^\pi \frac{d\sigma_-}{d\omega} \sin\theta d\theta. \quad (2)$$

Several measurements were made at each energy and absolute differential cross sections were obtained. All of the measurements agree both in shape and value to within 10%. However, several series of systematic errors are present: (1) effective

path length, (2) density determination, (3) measurements of the total beam, (4) angular resolution and integration, (5) energy spread of the scattered beam, and (6) detector calibration. The geometric path length has been corrected as discussed in Ref. 10 and the error estimated to be not more than 4%. The largest source of error in the present measurements arose from the target density determination, which is estimated to be $\pm 25\%$. The detector calibration was probably accurate to within $\pm 3\%$. The total error involved in the cross-section data is best expressed as the root-mean-square error, which is $\pm 26\%$.

III. EXPERIMENTAL RESULTS

Angular distributions for H⁻ formed in single collisions of H⁺ on Mg at several collision energies in the energy range 0.5 to 5.0 keV are shown in Fig. 2. Both energy and angle are given in the laboratory frame of reference. To obtain the absolute differential cross sections shown in this figure, the measured intensities were corrected for the channeltron detection efficiency as reported in Ref. 14. With this done, the differential cross sections were obtained using Eq. (1). As can be seen in Fig. 2, the H⁻ ions are formed mainly in the forward direction. From 1.0 to 5.0 keV the differential cross sections decrease monotonically with increasing angle with no visible structure. Some structure is found at energies lower than 1.0 keV which becomes more pronounced the lower the beam energy. Total cross sections, obtained by integrating the differential cross sections using Eq. (2), are shown in Fig. 3,

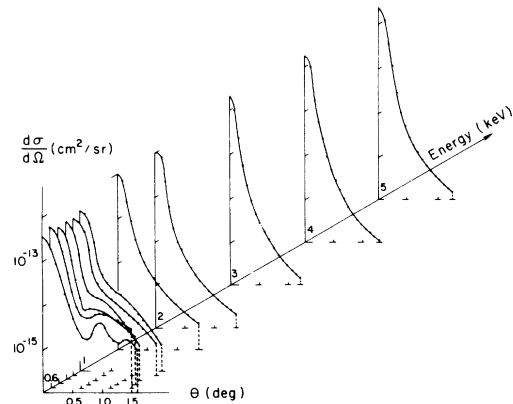


FIG. 2. Measured absolute differential cross sections for the process $H^+ + Mg \rightarrow H^- + Mg^{2+}$ for collision energies 0.5 to 5.0 keV.

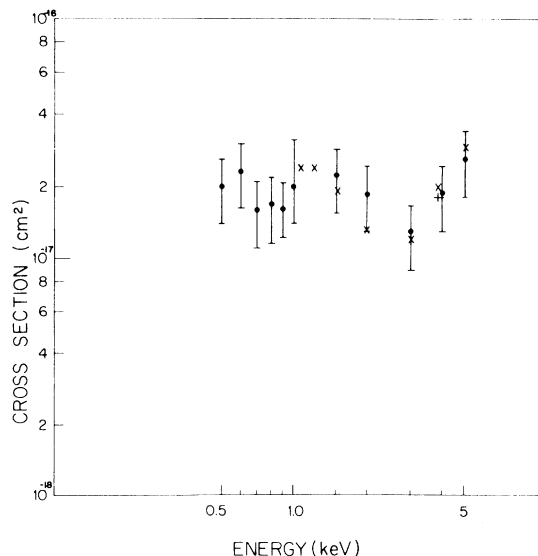


FIG. 3. Total cross sections. Solid black circles show the values obtained in the present work by integration of the measured differential cross sections shown in Fig. 2. Vertical bars give the experimental uncertainties. Total-cross-section measurements of Morgan and Eriksen in the energy range covered in the present work are shown by \times and the calculated total cross section is shown by $+$.

along with measurements of Morgan and Eriksen^{2,3} and the calculations of Olson and Liu.⁴ The results are seen to be in good agreement with the measurements of Morgan and Eriksen in the energy range common to the two experiments and are also in good agreement with the calculations.

IV. INTERPRETATION OF THE DATA

A. Scaling laws

The physics that governs a collision process can often be determined by demonstrating that all the cross-section data fall on a single universal curve predicted by some physical phenomenon. With that in mind, two different types of data plotting will be considered in this section which characterize two different types of physical phenomena.

(1) The first type of collision process to be considered is purely classical scattering (no diffraction or interference effects) by the adiabatic molecular potentials which determine a particular collision channel. A "channel" is nothing more than the complete specification of which molecular potential

applies at each segment of the trajectory. For purely elastic scattering, the force will be the same on inward and outward portions of the trajectory, while for an excitation process the potentials will not be the same on the inward and outward portions of the trajectory. All that is required is that the scattering force shall not be velocity dependent—that it be a function of the relative position vector only. When these conditions are met, it is possible to determine a classical deflection function $\theta(b, E)$, which depends on both impact parameter and collision energy, while $\tau = E\theta$ can be shown to be a function of impact parameter only. In this case, it has been demonstrated by Smith *et al.*⁷ that a universal curve is obtained when $\rho = \theta \sin\theta d\sigma/d\omega$ is plotted as a function of τ . The drawback of such a universal plot is that it does not exhibit the differential cross section itself and is almost useless in discussing the differential cross section in the vicinity of 0° scattering. An equivalent plot will now be developed which also yields a universal curve under the physical conditions just specified and which does exhibit the functional dependence of the differential cross section. For heuristic purposes, however, the ρ -vs- τ plot will be derived first.

The classical differential cross section is given by¹⁵

$$\frac{d\sigma}{d\omega} = \frac{b}{\sin\theta} \frac{db}{d\theta} \approx \frac{b db}{\theta d\theta}. \quad (3)$$

Multiplying Eq. (3) by θ^2 yields

$$\begin{aligned} \rho &\approx \theta^2 \frac{d\sigma}{d\omega} = \theta b db/d\theta = (E\theta) b db/d(E\theta) \\ &= \tau b db/d\tau. \end{aligned} \quad (4)$$

Since b is a function only of τ , the right-hand side of Eq. (4) depends only on τ . Thus ρ is a function of τ only.

A second function, which also depends only on τ while at the same time providing the functional dependence of the differential cross section, can be constructed by multiplying Eq. (3) by $1/E^2$. This equation then becomes

$$\frac{1}{E^2} \frac{d\sigma}{d\omega} = \frac{b db}{\tau d\tau} = f(\tau), \quad (5)$$

so that $E^{-2}d\sigma/d\omega$, when plotted as a function of τ , should yield a single universal curve for all collision energies.

(2) The second type of collision process here considered is that which follows from glory scattering, a diffraction phenomenon which occurs when the deflection function passes through zero at some fin-

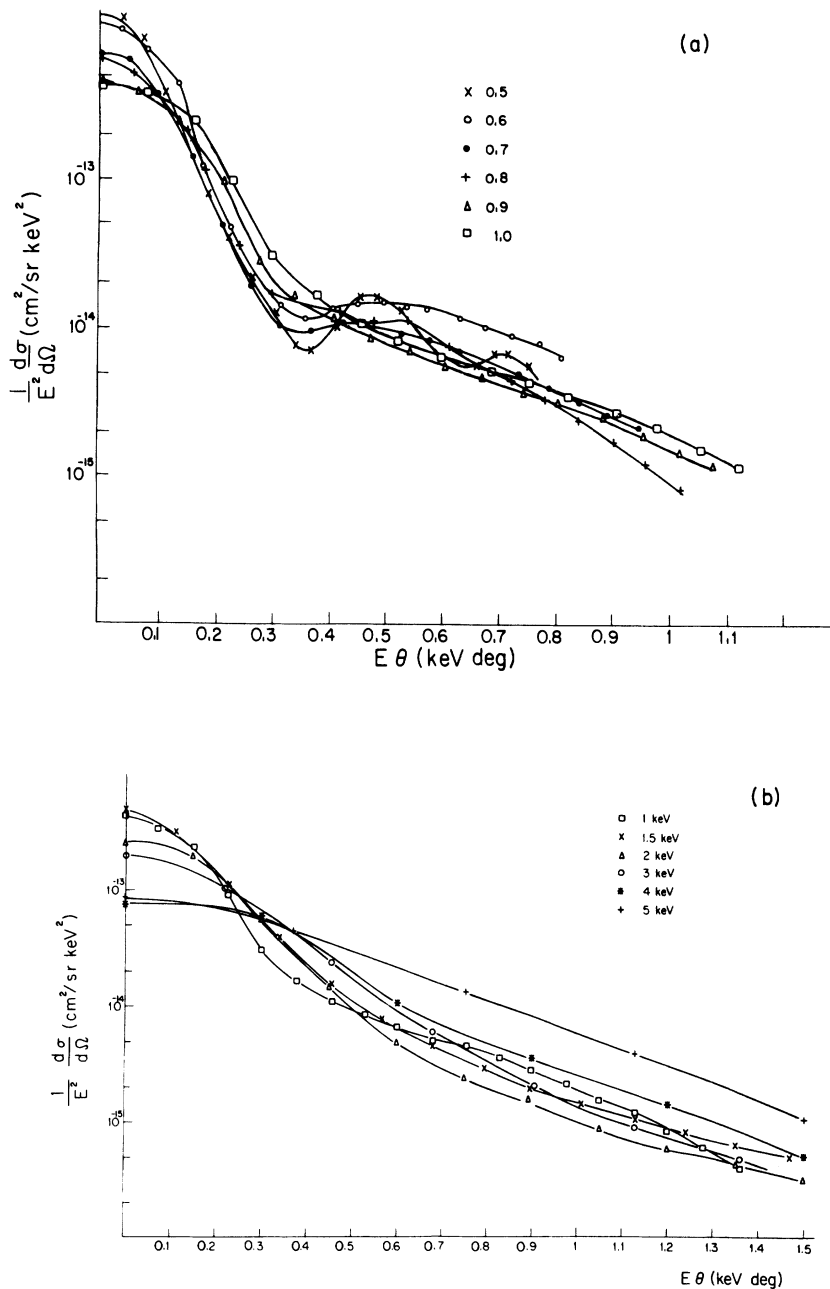
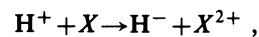


FIG. 4. Scaled differential cross sections. Differential cross sections of Fig. 2 are replotted in terms of the scaled variables $E^{-2}d\sigma/d\omega$ vs τ . Data at collision energies 0.5 to 1.0 keV are shown in (a) and the data at collision energies 1.0 to 5.0 keV are shown in (b).

ite impact parameter b_g . In 1959 Ford and Wheeler³ described a quantum-mechanical treatment of glory scattering based on single-channel potential scattering which assumed the deflection function θ to be a linear function of impact parameter b over the entire range of impact parameters which substantially contribute to the scattering amplitude in the vicinity of 0° deflection. Although

their model does not apply to an excitation process such as



which requires a multichannel theory, the Ford and Wheeler model is nevertheless of considerable help in understanding the data.

Ford and Wheeler demonstrate that if the deflec-

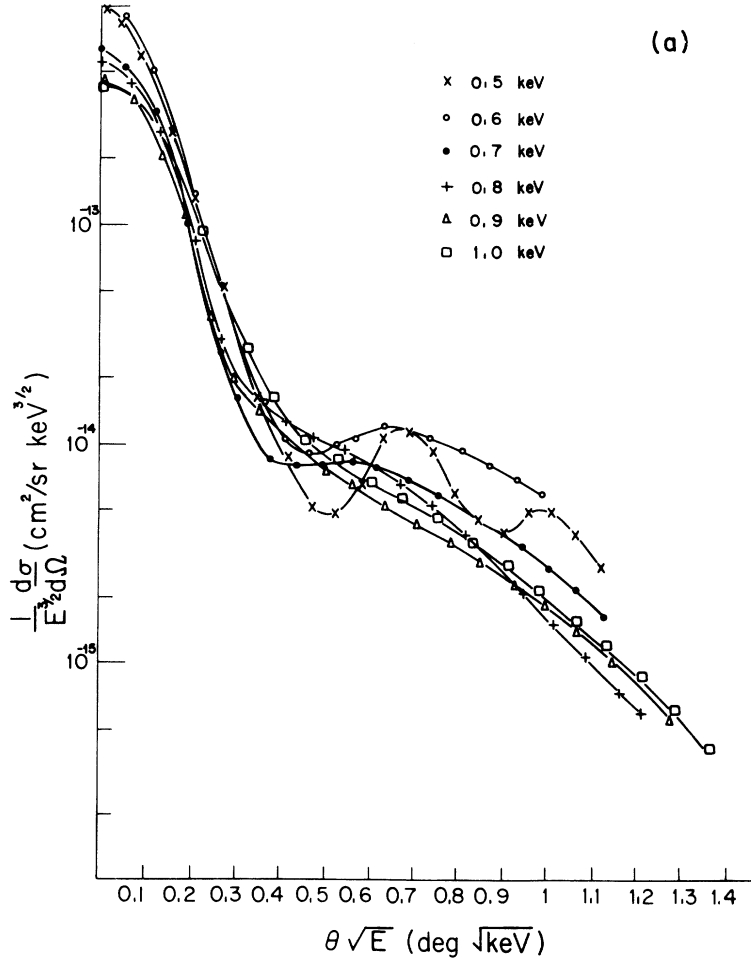


FIG. 5. Scaled differential cross sections. Differential cross sections of Fig. 2 are replotted in terms of the scaled variables $E^{-3/2}d\sigma/d\omega$ vs $E^{1/2}\theta$. Data at collision energies 0.5 to 1.0 keV are shown in (a) and the data at collision energies 1.0 to 5.0 keV are shown in (b).

tion function $\theta(b)$ for potential scattering is of the form

$$\theta = a(l - l_g) = ak(b - b_g), \quad (6)$$

where k is the relative momentum in a.u. and a is a constant which will be shown to be energy dependent, then the phase shift is given by

$$\delta_l = \frac{1}{4}a(l - l_g)^2 = \frac{1}{4}ak^2(b - b_g)^2 \quad (7)$$

and the differential cross section by

$$\frac{d\sigma}{d\Omega} = \frac{2\pi b_g^2}{|a|} J_0^2(kb_g \sin\theta). \quad (8)$$

Now the angle of scattering for a given impact parameter is not independent of energy. Rather, $\tau = E\theta$ is a function of b only, so that

$$E\theta = Eak(b - b_g) = f(b). \quad (9)$$

Therefore, Eak must be independent of energy, or

$$a = \alpha/E^{3/2}, \quad (10)$$

where α is a constant independent of energy. Thus, from (8),

$$E^{-3/2} \frac{d\sigma}{d\Omega} = \frac{2\pi b_g^2}{\alpha} J_0^2(kb_g \sin\theta). \quad (11)$$

For small angles the right-hand side is a function of $k\theta$ or $E^{1/2}\theta$ only. In other words, the Ford and Wheeler model predicts a universal curve, independent of incident energy, when the scaled cross sections $E^{-3/2}d\sigma/d\Omega$ are plotted as functions of $E^{1/2}\theta$ and, moreover, predicts a strong peak in the forward direction.

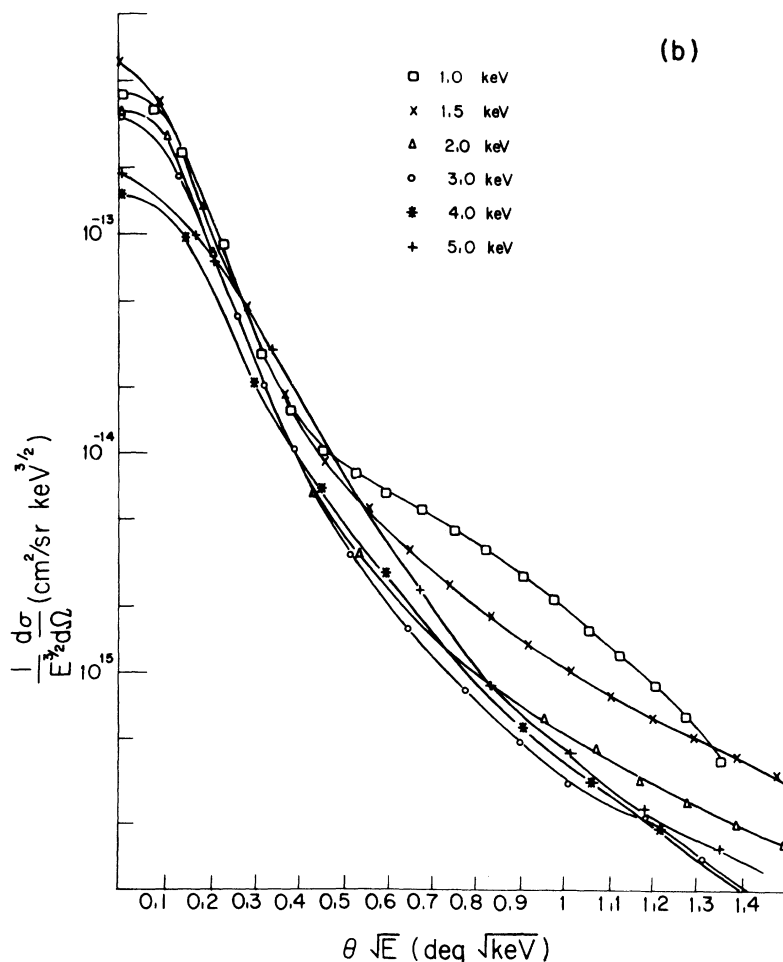


FIG. 5. (Continued.)

B. Plotting the data

In order to assess what happens during the collision, the experimental data of Fig. 2 are replotted in Figs. 4 and 5 in terms of the two sets of scaled variables described above. The scaled variables used in Fig. 4 are $E^{-2}d\sigma/d\omega$ vs τ , which would yield a universal curve for classical scattering in which both the scattering force and excitation amplitude are functions of the relative position vector \vec{R} only. (As functions of b and Z , rather than the scalar R , the scattering potential and state amplitude can be different on incoming and outgoing portions of the trajectory.) On the other hand, the scaled variables used in Fig. 5 are $E^{-3/2}d\sigma/d\omega$ vs $E^{1/2}\theta$, which would yield a universal curve for single-potential quantum-mechanical glory scattering.

The high-energy data clearly fall much closer to a single curve in Fig. 5 than they do in Fig. 4, thereby demonstrating that the physical phenomenon re-

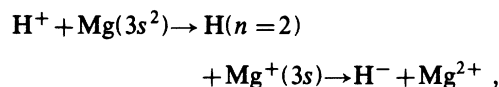
sponsible for the differential cross sections is glory scattering. The peak heights in Fig. 5 do not fall exactly on a single universal curve, but most, if not all, of this discrepancy is due to the fact that the Ford and Wheeler model is not strictly applicable to excitation processes. A more realistic partial-wave calculation, with an amplitude cutoff for impact parameters greater than the level crossing radius, does not yield a single universal curve, but a set of curves with the peak heights monotonically decreasing with increasing collision energy by just about the correct amount. The calculations based on a more realistic model will be presented elsewhere. Although the experimental curves exhibit the sharp 0° peak of glory scattering, they do not show the $J_0^2(kb_g \sin\theta)$ oscillations, which are beyond the instrumental angular resolution at all energies reported in this experiment. In order for the glory oscillations to be clearly resolved, the beam energy would have to be below 50 eV.

The low-energy data, in addition to exhibiting the glory peak, also show structure at larger angles. This structure falls much closer to a universal curve when plotted as a function of τ , as in Fig. 4, demonstrating that the process responsible for this structure is ordinary excitation at a level crossing sufficiently far removed from the glory region as to be essentially classical scattering.

C. Conclusions

In conclusion, the differential-cross-section measurements obtained here do not bear out the interpretations of Olson and Liu⁴ concerning the high-energy maximum in the total-cross-section data of Morgan and Eriksen.^{2,3} In the energy range from 2.0 to 5.0 keV, the angular distributions are quite smooth. They exhibit only the glory maximum for transitions taking place at 0° or near 0° scattering, with no hint at any transitions taking place at any nonzero value of τ . In particular, there is no hint at any transition on the repulsive wall of the potentials.

On the other hand, the low-energy differential-cross-section measurements do exhibit a τ -dependent structure characteristic of transitions taking place on the repulsive wall. However, the observed τ value is more indicative of the process



rather than the $\text{H} + \text{Mg}^+(4s)$ intermediate state suggested by Olson and Liu.

ACKNOWLEDGMENTS

This research was partially supported by joint grants from the National Science Foundation and Consejo Nacional de Ciencia y Tecnología: Grant No. NSF INT 79-05143, Grant No. PCNB-CONACyT 1367, and Grant No. PCCBNAL 790086. Two of the authors (I. A. and C. C.) wish to thank Dr. T. J. Morgan for helpful discussions at the beginning of the experiment. The help of R. Castillo during the acquisition and reduction of the data is appreciated.

¹K. H. Berkner, R. V. Pyle, and J. W. Stearns, *Phys. Rev.* **178**, 248 (1969).

²T. J. Morgan and F. J. Eriksen, *Phys. Lett.* **66A**, 198 (1978).

³T. J. Morgan and F. J. Eriksen, *Phys. Rev. A* **19**, 1448 (1979).

⁴R. E. Olson and B. Liu, *Phys. Rev. A* **20**, 1366 (1979).

⁵G. A. L. Delvigne and J. Los, *Physica* **67**, 166 (1973).

⁶K. W. Ford and J. A. Wheeler, *Ann. Phys. (N.Y.)* **7**, 259 (1959).

⁷F. T. Smith, R. P. Marchi, and K. G. Dedrick, *Phys. Rev.* **150**, 79 (1966).

⁸I. Alvarez, C. Cisneros, and A. Russek, *Phys. Rev. A* **23**, 2340 (1981).

⁹L. Wahalin, *Nucl. Instrum. Methods* **27**, 55 (1964).

¹⁰C. Cisneros, I. Alvarez, C. F. Barnett, and J. A. Ray,

Phys. Rev. A **14**, 76 (1976).

¹¹N. Nesmeianov, *Vapor Pressures of Elements*, translated and edited by J. I. Carasso (Academic, New York, 1961).

¹²R. R. Hultgren, R. L. Orr, P. D. Anderson, and K. K. Kelley, *Selected Values of Thermodynamic Properties of Metals and Alloys* (Wiley, New York, 1968). Present data taken from supplement issued in 1970.

¹³R. R. Hultgren, P. D. Olsai, D. T. Hawkins, M. Gleiser, K. K. Kelley, and D. D. Wagman, *Selected Values of Thermodynamic Properties of Elements* (American Society for Metals, Cleveland, 1973).

¹⁴D. H. Crandall, J. A. Ray, and C. Cisneros, *Rev. Sci. Instrum.* **46**, 562 (1975).

¹⁵H. Goldstein, *Classical Mechanics* (Addison-Wesley, Cambridge, Mass., 1953), pp. 81-82.